Where is the missing felsic crust of Greater Indian continent?

Lifei Zhang (lfzhang@pku.edu.cn)
Peking University https://orcid.org/0000-0002-5118-8811
Yang Wang
Peking University
Zhong-Hai Li
University of Chinese Academy of Sciences https://orcid.org/0000-0003-1968-5129

Physical Sciences - Article

Keywords: continental crust, felsic crust, Greater India

Posted Date: July 9th, 2021

DOI: https://doi.org/10.21203/rs.3.rs-227521/v1

Where is the missing felsic crust of Greater Indian continent?

Yang Wang[1], Lifei Zhang[1*], Zhong-Hai Li[2*]

[1]*Key Laboratory of Orogenic Belts and Crustal Evolution, School of Earth and Space Science, Peking University, Beijing 100871, China*

[2]*Key Laboratory of Computational Geodynamics, College of Earth and Planetary Sciences, University of Chinese Academy of Sciences, Beijing 100049, China*

[*] Corresponding: *L.F.Z (lfzhang@pku.edu.cn) and Z.H.L (li.zhonghai@ucas.ac.cn).*

Abstract

According to the plate tectonics theory, continental crust (CC), especially the felsic upper and middle continental crust (UCC and MCC), cannot subduct due to its buoyancy. Therefore, most, if not all, of the felsic crustal mass will be preserved in continental collision zones or eroded by the surface process. Consequently, the continent-continent convergence is generally slower and more short-lived than oceanic plate subduction. However, the long-duration, fast convergence, and imbalance of crustal mass in the India-Asia collisional system challenge the classical rules of plate tectonics. Systematic compilation and calculations indicate ~20-47% of the felsic crust in Greater India is missing during collision. Based on the phase equilibria modeling and density calculations, we explore the pressure-temperature-dependent density evolutions of UCC and MCC and demonstrate they are denser than the surrounding mantle at P >7-8 GPa when the phase transition from coesite to stishovite occurs. The phase equilibria induced density evolution is further integrated into the thermo-mechanical model, which confirm the deep subduction of Greater Indian continent with its felsic UCC and MCC. Analytical studies of the slab-pull forces in the subduction zone indicate the Greater Indian continent can subduct spontaneously under its own negative buoyancy when it is dragged to a depth of ~170 km by the preceding oceanic slab. The great slab-pull force, induced by the negative buoyancy of UCC and MCC below 170 km, not only contributes to the long-lasting fast convergence between India and Asia, but also explains the crustal mass imbalance during the Himalayan orogeny.

Introduction

Knowing how and how much felsic crust was consumed during collision play a critical role in addressing the key problem in continental dynamics. By considering crustal thickening, surface erosion and tectonic escape, previous studies revealed a loss of ~50% of the pre-collisional crustal mass between India and Asia in the archetype of active collisional systems, the Himalayas[1]. The Greater Indian Oceanic Basin hypothesis[2] and the subduction of mafic Indian lower continental crust (LCC) after UCC scrapoff[3] have been invoked to explain the loss of crust. However, it remains a contentious issue for the missing of (felsic) crustal mass of Great Indian Continent. Another puzzling issue is about the driving force for the unusually fast and long-lasting convergence (18–4 cm/yr) of Indian-Asian continental collision. Many hypotheses have been proposed: (1) the negative buoyancy of the Greater Indian lithosphere without UCC[3], (2) the push of the Indian Ocean ridge[4], and (3) the drag from the neighboring oceanic slab pull beneath Burma[5]. However, these existing hypotheses and models have great difficulty in explaining the multiple facts, including the imbalance of crustal mass, the rapid convergence rate and the long collisional period. A key problem is that all the aforementioned explanations assumed that the felsic UCC and MCC are buoyant, but ignored the effect of metamorphic phase transformation on their density under ultrahigh pressure conditions. Below, we will firstly evaluate the mass deficit of felsic crust in Greater Indian Continent, and then explore the density evolution of CC and the effect of metamorphic densification on continental subduction evolution using both a petrological-thermo-mechanical model and a simplified analytical model.

Mass imbalance in the felsic crust of Greater Indian Continent (GIC)

Previous calculations of the crustal mass deficit have focused on the whole India-Asia collisional orogen[1,6,7]. In order to better understand the behavior of felsic crust during continental subduction, we focus on the GIC and reassess its mass balance of UCC/MCC. Greater India is the part of Indian plate that has been consumed since the onset of Cenozoic continental subduction and collision. However, the extent of GIC from reconstructions varies greatly from ~900 km to ~2600 km (Extended Data Table 1). Using the relatively well-constrained pre-collisional data of Greater India[1,6,7,8,9] and the global average UCC and MCC crustal thickness of 23 km[10], we derive the volume of Greater Indian felsic crust, ranging from $7.13\pm0.69\times10^7$ km^3 to $10.81\pm1.15\times10^7$ km^3 (Extended Data Table 2). After collision, the Greater India-derived continental felsic crust is mainly preserved in the Himalaya fold-thrust belt [11]. Besides, the seismic reflection profiles indicate that the Indian-affinity UCC/MCC is rarely transported northwards beyond the Yarlung Zangbo suture or added into the Lhasa and Qiangtang terranes[12], which means the modern Himalaya thrust belt conserve the major pre-collisional Greater Indian UCC/MCC except for the surface erosion and lateral extrusion. The Himalaya thrust belt occupies an area of ~0.83×10^6 km^2 with an average crustal thickness of 57 km[6]. Even under an extreme assumption that the entire Himalayan crust is felsic, the volume of felsic crust in the Himalaya domain is only 4.73×10^7 km^3. On the other hand, we use an average erosion rate of about 0.25 km/Ma since 50 Ma[13] to obtain the erosional volume flux in GIC of 10.38×10^6 km^3, which is consistent with the previous estimate of erosional volume of ~10.4×10^6 km^3 in Himalaya[6]. Another possible contribution in estimating the mass balance of GIC is the lateral extrusion of crustal blocks. However, the southeastward material extrusion generally occurred with the deformed Asia domain[14], whereas the escaped felsic crust of GIC is negligible and thus ignored in our evaluation. Therefore, if there is no subduction of felsic crust, the UCC/MCC

crustal volume of GIC must balance the net volume of UCC/MCC in the present Himalaya and that being eroded. However, the final results (Extended Data Table 2) reveal the missing GIC felsic crust of 1.36×10^7 km^3 to 5.04×10^7 km^3, or ~20% to 47% of the pre-collisional UCC/MCC, based on different reconstructions of GIC[1,6,7,8,9]. It is worth noting that the estimate is just the lower limit of mass deficit due to overestimate of the UCC/MCC thickness in the present Himalaya. These results may imply that significant amount of Greater Indian felsic crust is subducted and recycled into the mantle.

Phase transition-induced densification of subducting continental crust

The density of CC in the subduction channel plays an essential role in controlling the continental deep subduction or not. Here, we use Perple_X to compute the phase relations and densities for the average UCC, MCC, and LCC compositions[10] (Extended Data Table 3) in the pressure (P)–temperature (T) range of 0–24 GPa and 0–1800 ºC. The density of UCC lies in the range of 2416.98–4381.60 kg/m^3 (Fig. 1 and Extended Data Fig. 1a). Within the P–T range of interest (2–10 GPa, 400–1800 ºC), the P–T–density (ρ) diagram of UCC (Fig. 1) reveals four major density jumps. The first jump, with an increase of density by up to 75–90 kg/m^3 at ~2.7 GPa, is caused by the phase transition from quartz to coesite. The phase transitions of feldspars at 5.5–7 GPa, i.e. microcline –> K-wadeite or plagioclase-kalsilite –> K-wadeite, result in the second density jump (by 120 kg/m^3), which brings the UCC density closer to that of the mantle at the same depth. The third dramatic density jump by 380–400 kg/m^3 occurs at 7–9 GPa, after which UCC becomes approximately 400 kg/m^3 denser than the surrounding mantle and can provide a large driving force for continental subduction. It thus challenges the classical perspective that the CC, especially UCC, is always buoyant in the subduction channel. Finally,

the phase transition of K-wadeite –> K-hollandite (Liebermannite) occurs at 8–9 GPa, with the fourth major density jump of 80–90 kg/m^3.

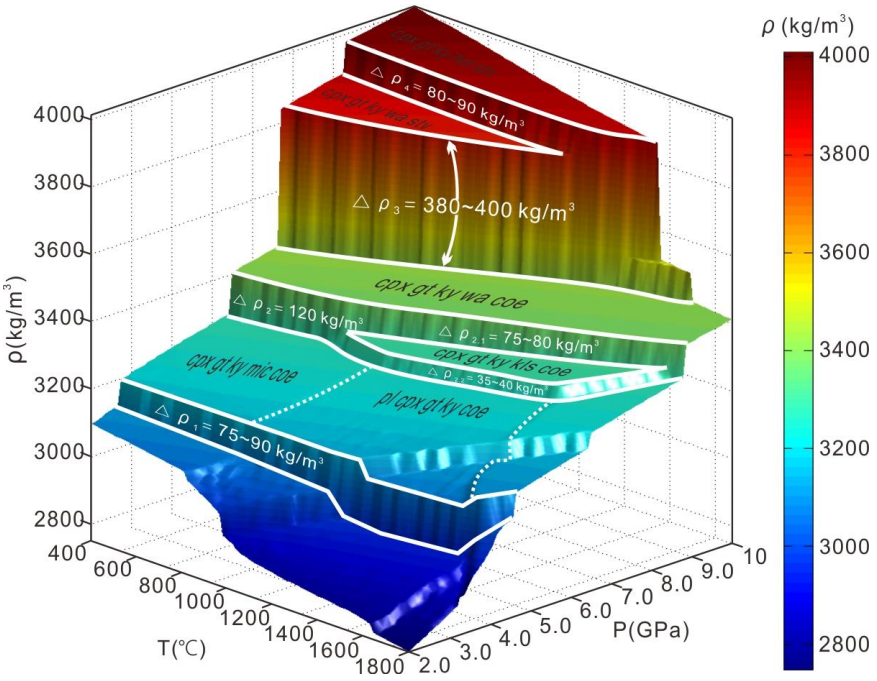

Fig. 1 | The 3D density evolution of the chosen average UCC composition. The white lines denote the major metamorphic phase transitions controlling the density increase of UCC. The four major density jumps with characteristic values are shown in white. The stable mineral assemblages are shown in black with the meanings of mineral abbreviations in the Methods.

In order to verify the new phase diagram with P-T-dependent density evolutions, we further extract the density profiles of UCC along three different P-T paths in the cold, normal and hot subduction channels, respectively. The results are comparable with previous experimental studies[15,16,17] (Extended Data Fig. 2). On the other hand, the density evolution of MCC is comparable to that of UCC (Extended Data Fig. 1a, b) due to their similar bulk compositions. Similarly, the density of mafic LCC is comparable to that of MORB (Extended Data Fig. 1c, d).

The sensitivity tests with different crustal compositions[10] (Extended Data Table 4) are further conducted and compared with the reference model (Extended Data Fig. 3 and 4). The density profiles of UCC along a typical subduction P-T path with different bulk-rock compositions indicate that the higher Si content reduces the density of UCC at P < ~8 GPa, but increases its density at P > ~8 GPa (Extended Data Fig. 3), with the density reversal mainly due to the phase transition of coesite –> stishovite. The density variation induced by different Si content is about -2.79%~3.53% (Extended Data Fig. 4). On the other hand, the effects of variable X_{Mg} [MgO/(MgO+FeO)], X_{Al} [Al_2O_3/(Al_2O_3+MgO+FeO)] and X_{Ca} [CaO/(CaO+MgO+FeO+Na_2O)] on the density evolution are negligible, with even low density variations of -0.63%~0.31%, -0.37%~0.54%, -0.32%~0.35%, respectively (Extended Data Fig. 4). Consequently, the possible composition variation of UCC does not play a significant role in the density evolution and thus will not affect the general perspective of this study.

Integrated petrological-thermo-mechanical modelling of continental subduction

In order to better understand the role of phase transition-induced density evolution on the dynamics of continental subduction, the P-T-dependent density database (see Methods) is further integrated into a thermo-mechanical numerical model using 2-D finite difference code I2VIS[18,19]. The original model consists of Greater Indian and Asian continents on the left and right sides, respectively, with a section of Neo-Tethyan oceanic plate in between (Fig. 2a). The subducting plates are pushed internally by a prescribed velocity of 10 cm/yr for 7 Myrs, with a total convergence of 700 km (Fig. 2b). It leads to a snapshot with the beginning of continental collision, after which the prescribed constant convergent velocity is cancelled, leaving the continental subduction driven purely by the negative buoyancy of the slab.

In the following study, the initial collision scenario (Fig. 2b) is employed as the initial model. Two different models with contrasting density evolutions are further applied and compared. In Model-I, the density is linearly dependent on pressure and temperature, but does not include any phase transition. In contrast, Model-II incorporates our calculated density database with multiple phase transitions and density jumps (Extended Data Fig. 1). The results of Model-I (Fig. 2c, d) show that the continental lithosphere subducts with a low convergence velocity of ~1 cm/yr for about 2 Myrs (Fig. 2h) dragging by the preceding oceanic slab. The accumulated buoyancy of subducted continental crust resists and finally terminates the subduction process, with the oceanic slab breakoff occurring at the end. The results of Model-II (Fig. 2e, f) show that the continental plate is firstly dragged into mantle by the subducted oceanic slab, with a high velocity of ~8.5 cm/yr (Fig. 2h). The continuous subduction of low-density felsic crust decreases the convergence velocity gradually, to a low value of ~ 4 cm/yr (Fig. 2h). However, the deep continental subduction leads to phase transitions of silicates in the felsic crust and results in remarkable density increase (Fig. 2g). Consequently, the increasing negative buoyancy of continental plate contributes to faster subduction with a peak convergent velocity of ~12 cm/yr (Fig. 2h). During collision, a large portion of felsic crust is gradually scraped off and enters the orogenic system of Himalaya fold-thrust belt. Meanwhile, a certain amount of UCC/MCC subducts with the sinking slab and is recycled into the deep mantle (Fig. 2f). The cumulative recycled volume of felsic crust is calculated to be ~26% of the initial felsic crust in the left continent at the model time of 20 Ma when the entire subducting continental plate is consumed (Fig. 2h).

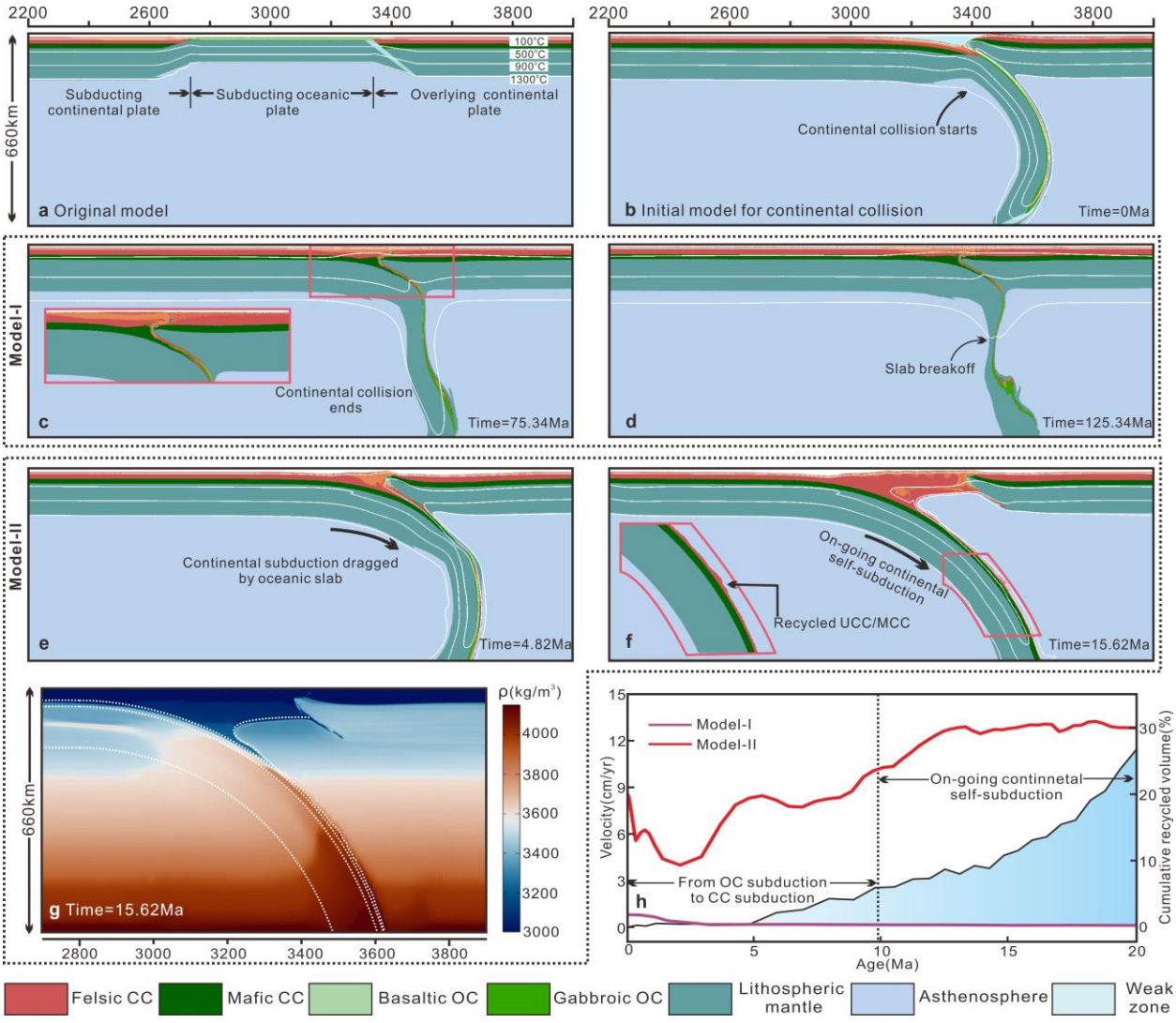

Fig.2 | The model results of continental subduction with two different density evolutions. a, Original model configuration with a subducting continental plate, an overlying continental plate on both side and a subducting oceanic plate in between. The subducting plates are pushed internally by a constant velocity of 10 cm/yr for 7 Myrs. b, The beginning of continental collision after 7 Myr with a total convergence of 700 km. This snapshot is used as the initial model for following study, which is pure density-driven free subduction without any pushing. Two different continental density structures are further applied in Model-I and Model-II. c, d, Evolution of Model-I without phase transition. The inset figure in (c) indicates the ending of

continental convergence. e, f, Evolution of Model-II with phase transition and metamorphic densification. The inset figure in (f) shows the continuous subduction of a part of felsic crust. g, The density structure of continental subduction zone in (f). h, The convergence velocity evolutions of Model-I and Model-II (left axis) and the accumulated recycled volume of subducted felsic continental crust in Model-II (right axis) which is calculated as

$$\text{Cumulative recycled volume} = \frac{Subducted\ felsic\ continntal\ crust\ beneath\ 150km}{Initial\ felsic\ continetal\ crsut\ in\ subudcted\ contiental\ plate}.$$

It is worth noting that the resultant convergent velocity in the simple numerical model (Fig. 2h) is not aimed to match the exact kinematic evolution of natural Indian-Asian collision system, because the latter has a complex tectonic evolution history and differential subduction in eastern and western Himalayas[11,20]. However, the integrated petrological-thermo-mechanical model indicates that the phase transition-induced densification of deeply subducted felsic crust could be involved to explain not only the mass deficit of GIC, but also the driving force for long-lasting Indian-Asian convergence. In addition, the multi-stage reduction of India-Asia convergence velocity[6,20] may be caused by the multiple breakoff of subducted continental lithosphere, although it is not reconciled in the current simple model.

Analytical examinations of continental slab pull with metamorphic densification

The phase transition-induced density evolution is further coupled with a typical *P–T* structure of subduction zone[21] (Fig. 3a and see Methods), which shows dramatic density changes of the subducted CC, especially UCC/MCC (Fig. 3b), due to major phase transitions, e.g., quartz → coesite → stishovite (2633 kg/m^3 → 2910 kg/m^3→ 4290 kg/m^3) and kalsilite/microcline → K-wadeite → K-hollandite (2600/2560 kg/m^3→ 3110 kg/m^3→ 3890 kg/m^3). The UCC at the top of the slab experiences more intense conductive heating and reaches the great density jump of

about +350 kg/m^3 at 240–250 km; the MCC is slightly colder due to the less conductive heating which leads to a similar density jump at a relatively shallow depth due to the positive Clapeyron slope of coesite → stishovite. After the transformation from K-wadeite to K-hollandite in the depth range of 240–270 km, the whole CC, especially UCC and MCC, is about 450 kg/m^3 denser than the surrounding mantle and can thus provide a great slab pull force.

By analytical model of density evolution in continental subduction zone, we reevaluate the slab pull of OC, CC, and the entire slab (OC + CC) (F_{OC}, F_{CC} and F_{total}, respectively) above 660-km discontinuity (660D), from oceanic subduction to continental collision (see Methods).The result (Fig. 3c) shows that F_{OC} is largest at the beginning with a value of up to 1.0×10^{13} N/m, when the OC is completely subducted and continental collision starts. Assuming there is no breakoff between OC and CC, the total body force F_{total} is always positive ($F_{total} > 0$). This means that even if the UCC and MCC have not been scraped off, the entire CC can still be dragged by the preceding oceanic slab into the mantle, even to the bottom of mantle transition zone (MTZ). With continuous subduction, the residual oceanic slab above 660D is shorter and shorter and finally F_{OC} goes down to zero (Fig. 3c). In contrast, F_{CC} firstly decreases to a minimum of $-1.6 \times 10^{12}\mathrm{N/m}$ at a depth of ~90 km and then gradually increases to a high value of $4.0 \times 10^{13}\mathrm{N/m}$ (Fig. 3c) due to the eclogitization of mafic LCC and the phase transformations of silicates in UCC and MCC. The high F_{CC} is in the same order of magnitude with the downward gravitational body force of the descending oceanic lithosphere caused by thermal contraction and elevation of the olivine phase change (F = 3~5×10^{13} N/m), which was previously regarded as the dominant force driving plate tectonics[22]. Therefore, after considering the metamorphic phase transition and densification, the negative buoyancy of CC (without slab breakoff) is sufficient to sustain the fast and continuous convergence between the Indian and

Asian plates. Further on, the slab pull forces of UCC, MCC and LCC are calculated separately, in order to understand their relative contributions to the entire F_{CC} (Fig. 3d). The result shows the maximum driving forces of UCC, MCC, and LCC are 9.0×10^{12} N/m, 1.2×10^{13} N/m and 2.4×10^{13} N/m, respectively, and account for 20%, 26%, and 54% of F_{CC}. Thus, with the metamorphic phase transition and induced densification, F_{CC} is in the same order of magnitude with F_{OC}.

In the above calculations, the whole continental plate is presumed to subduct together, which is however not the case for the natural Earth, because a large portion of felsic crust could be scraped off when entering the subduction channel which, for example, contributes to the formation of Himalaya range in the Indian-Asian collision system. Thereby, we further calculate the slab pull of subducted CC after different thicknesses of UCC/MCC being scraped off (Extended Data Fig. 5a). The results show a clear positive correlation between the slab pull and the degree of scraping (Extended Data Fig. 5b). For example, if ~20% to 47% of the pre-collisional UCC/MCC is recycled into the mantle, i.e. the possible case for GIC, the slab pull of subducted GIC ranges from ~2.93×10^{13} N/m to ~3.38×10^{13} N/m which is high enough to drive continuous subduction.

The metamorphic phase transition and densification offers a key to re-exploring the fate of subducted CC. At the beginning of continental collision, the subduction of buoyant CC into the mantle levels must be assisted by the drag of the high-density oceanic slab. When the CC reaches a critical depth of approximately 170 km (D1 in Fig. 3d), it is negatively buoyant after the major phase transitions, i.e. $F_{CC} > 0$. Accordingly, if the breakoff of the subducted slab occurs below 170 km, the negative buoyancy of the entire CC can still drive the continuous continental subduction. In contrast, a slab breakoff at shallower depth would impede further subduction of CC. On the other hand, if the continental plate subducts continuously to about 320 km (D2 in

Fig. 3d), the UCC layer itself is negatively buoyancy. This means that even if the UCC is decoupled from the subducting slab, it can still sink by itself to the bottom of MTZ.

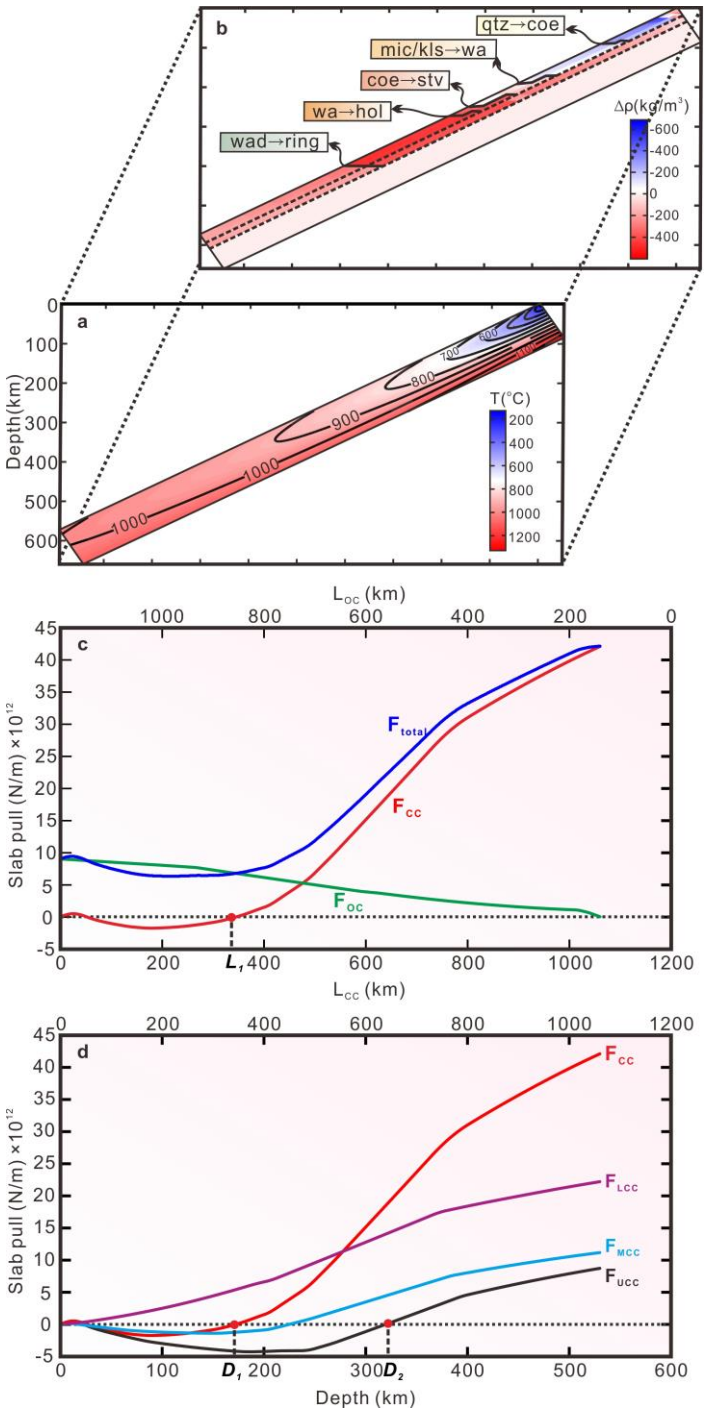

Fig.3 | The density variation and slab pull of continental crust with metamorphic densification. a, The thermal structure of the subducted continental lithosphere above 660D. The

thermal structure is obtained from the analytical solution of Davies et al. (1999)[20] (see Methods), where the mantle potential temperature $T_1 = 1325$ °C, the initial minimum temperature on the slab $T_0 = 100$ °C, the lithosphere thickness $h = 100$ km, the thermal diffusivity $\kappa = 10^{-6} m^2 s^{-1}$, the subduction angle $\theta = 30°$, the convergence velocity $v = 5$ cm/yr, and the initial thickness of the boundary layer in the mantle wedge $d = 20$ km. b, The density variation of the subducted continental lithosphere above 660D.The dashed lines are the interfaces between MCC, LCC, and LM and the solid lines represent significant density jumps caused by phase transition. c, The slab pull of subducted CC, OC, and the entire slab along the prescribed subduction channel above 660D during the transition from oceanic subduction to continental collision, where L_{CC} is the length of the subducted CC increasing from 0 to $\frac{660}{\sin\theta}$ km (θ=30° is the prescribed subduction angle), L_{OC} is the length of the residual subducted OC above 660D ($L_{OC} = \frac{660}{\sin\theta} - L_{CC}$). d, The slab pull of CC, UCC, MCC, and LCC during the continental subduction, indicating the contributions of F_{UCC}, F_{MCC}, and F_{LCC} to F_{CC}. For $D_1 \approx 170$ km, $F_{CC} = 0$ N/m, indicating the body force of the entire CC becomes greater than zero when the continental slab sinking deeper than ~170 km; and for $D_2 \approx 320$ km, $F_{UCC} = 0$ N/m, indicating the body force of the entire UCC become greater than zero when the UCC sinking deeper than ~320 km. The slab pull evolutions of CC with variable amount of crustal materials scraped off during subduction and different subduction angles are shown in Extended Data Fig. 5 and 6, respectively.

Deep subduction and recycling of felsic crust in Greater India and globally

Metamorphic rocks of the India-Asia collision system provide crucial insights into deep subduction processes. In the Tso Morari and Kaghan massifs, the coesite-bearing eclogites indicate the Indian continent has subducted to a minimum depth of 90 km[23, 24]. Moreover,

according to conventional geothermobarometry, the ultra-high-pressure (UHP) coesite-bearing eclogites in Tso Morari show a peak pressure of around 44-48 kbar at 560-760 ºC and indicate a deep subduction depth of about 160 km[25]. This is approaching the critical depth (i.e. 170 km), below which CC can self-subduct. In addition, the Oligocene-Miocene ultrapotassic rocks and the latest Eocene Quguosha gabbros in the Lhasa block (i.e. the overriding plate of Indian subduction) originated from relatively deep levels, with exceptional depletion in Nb-Ta-Ti, significant enrichment in LILE, LREE and Sr-Nd isotopic composition; these geochemical signatures are generally considered to result from the addition of a large amount of sediment derived from the subducted Indian UCC to the mantle[26, 27]. The deep subduction of Indian UCC and MCC could have provided abundant potassium for the K-rich magmatism widespread in the Lhasa terrane from west to east. Additionally, many seismic tomographic images reveal that Indian lithosphere subducted to mantle depths[6, 28, 29, 30], although it is challenging in identifying subducted felsic crust from Indian lithosphere due to the limit of tomographic resolution.

The combined thermodynamic phase transition, thermo-mechanical numerical modelling and slab pull force analyses imply that the deep subduction of CC in continental collision belts may play a crucial role in the global crustal recycling and the reconstruction of CC growth and preservation throughout geological history[31]. On the other hand, abundant input of felsic crust into deep mantle contributes significantly to the mantle properties and geochemical heterogeneities [32]. Some recognized mineralogical evidences in global, well-studied UHP terranes also demonstrate the subduction and exhumation of CC from deep levels of the upper mantle (Extended Data Table 7 and Fig. 7). It is noteworthy that the exhumed rocks from the deeper upper mantle, i.e. > 8 GPa, is generally rare, which should be accompanied with and dragged by other buoyant materials; this problem requires further studies.

Online content Methods, along with any additional Extended Data display items and Source Data, are available in the online version of the paper; references unique to these sections appear only in the online paper.

REFERENCES CITED

1. Ingalls, M., Rowley, D. B., Currie, B. & Colman, A. S. Large-scale subduction of continental crust implied by India-Asia mass-balance calculation. *Nat. Geosci.* **9**, 848-853 (2017).
2. van Hinsbergen, D. J. J. et al. Greater India Basin hypothesis and a two-stage Cenozoic collision between India and Asia. *Proc. Natl Acad. Sci. USA* **109**, 7659–7664 (2012).
3. Capitanio, F. A., Morra, G., Goes, S., Weinberg, R. F. & Moresi, L. India-Asia convergence driven by the subduction of the greater Indian continent. *Nat. Geosci.* **3(2)**, 136-139 (2010).
4. Chemenda, A. I., Burg, J. P. & Mattauer, M. Evolutionary model of the Himalaya–Tibet system: geopoem: based on new modelling, geological and geophysical data. *Earth Planet. Sci. Lett.* **174(3)**, 397-409 (2000).
5. Li, C., van der Hilst, R. D., Meltzer, A. S. & Engdahl, E. R. Subduction of the Indian lithosphere beneath the Tibetan Plateau and Burma. *Earth Planet. Sci. Lett.* **274**, 157–168 (2008).
6. Replumaz, A., Negredo, A. M., Guillot, S., Beek, P. V. D. & Villaseñor, A. Crustal mass budget and recycling during the India/Asia collision. *Tectonophysics* **492(1-4)**, 99-107 (2010).
7. Yakovlev, P. V. & Clark, M. K. Conservation and redistribution of crust during the Indo-Asian collision. *Tectonics* **33,** 1016–1027 (2014).
8. Meng, J., Gilder, S. A., Wang, C., Coe, R. S., Tan, X., Zhao, X. & He, K. Defining the Limits of Greater India. *Geophys. Res. Lett.* **46,** 4182–4191 (2019).
9. Gibbons, A. D., Barckhausen, U., Bogaard, P. V. D., Hoernle, K., Werner, R., Whittaker, J. M. & Müller R. D. Constraining the Jurassic extent of Greater India: Tectonic evolution of the West Australian margin, *Geochem. Geophys. Geosyst*. **13,** Q05W13 (2012).
10. Rudnick, R. & Gao, S. 4.1- Composition of the Continental Crust. *Treatise on Geochemistry* Volume 4 (2014).
11. van Hinsbergen, D. J. J., Lippert, P. C., Li, S., Huang, W. & Spakman, W. Reconstructing greater india: paleogeographic, kinematic, and geodynamic perspectives. *Tectonophysics* **760**, 69-94 (2019).

12. Gao, R., Lu, Z., Klemperer, S. L., Wang, H., Dong, S., Li, W. & Li, H. Crustal-scale duplexing beneath the Yarlung Zangbo suture in the western Himalaya. *Nat. Geosci.* **9(7),** 555-560 (2016).
13. Richter, F. M., Rowley, D. B. & Depaolo, D. J. Sr isotope evolution of seawater: the role of tectonics. *Earth Planet. Sci. Lett.* **109(1-2)**, 11-23 (1992).
14. Li, S., Advokaat E. L., van Hinsbergen, D. J. J., Koymans, M., Deng, C. & Zhu, R. Paleomagnetic constraints on the Mesozoic-Cenozoic paleolatitudinal and rotational history of Indochina and South China: Review and updated kinematic reconstruction. *Earth-Sci. Rev.* **171,** 58-77 (2017).
15. Irifune, T., Ringwood, A.E., & Hibberson. W.O. Subduction of continental crust and terrigenous and pelagic sediments: an experimental study. *Earth Planet. Sci. Lett.* **126(4),** 351-368 (1994).
16. Ishii, T., Kojitani, H., Akaogi, M. High-pressure phase transitions and subduction behavior of continental crust at pressure-temperature conditions up to the upper part of the lower mantle. *Earth Planet. Sci. Lett.* **357-358,** 31-41 (2012).
17. Nishi, M. et al. High-pressure phase transitions of anorthosite crust in the Earth's deep mantle. Geosci. Front. 9, 1859-1870 (2018).
18. Li, Z. H., Gerya, T., & Connolly, J. A. D. Variability of subducting slab morphologies in the mantle transition zone: Insight from petrological‐thermomechanical modeling. *Earth-Sci. Rev.* **196,** 102874 (2019).
19. Gerya, T. V. Introduction to numerical geodynamic modelling. Cambridge University Press (2010).
20. Parsonsa, A. J., Hosseinia, K., Palin, R. M. & Sigloch, K. Geological, geophysical and plate kinematic constraints for models of the India-Asia collision and the post-Triassic central Tethys oceans. *Earth-Sci. Rev.* 103084 (2020). https://doi.org/10.1016/j.earscirev.2020.103084
21. Davies, J. H. Simple analytic model for subduction zone thermal structure. *Geophys. J. Int.* **139(3)**, 823–828 (1999).
22. Turcotte, D. L. & Schubert, G. Geodynamics -3rd edition (2014).
23. O'Brien, P. J., Zotov, N., Law, R., Khan, M. A. & Jan, M. Q. Coesite in Himalayan eclogite and implications for models of India-Asia collision. *Geology* **29(5)**, 435-438 (2001).
24. Mukherjee, B., Sachan, H., Ogasawara, Y., AtsumiMuko & Nobuhiro Yoshioka. Carbonate-bearing UHPM rocks from the Tso-Morari region, Ladakh, India: petrological implications. *Int. Geol. Rev.* **45(1)**, 49-69 (2003).

25. Wilke, F. D. H., O'Brien, P. J., Schmidt, A. & Ziemann, M. A. Subduction, peak and multi-stage exhumation metamorphism: traces from one coesite-bearing eclogite, Tso Morari, western Himalaya. *Lithos,* **231(11)**, 77-91 (2015).

26. Ma et al. Subduction of Indian continent beneath southern Tibet in the latest Eocene (~ 35 ma): Insights from the Quguosha gabbros in southern Lhasa block. *Gondwana Res.* **41**, 77-92 (2017).

27. Guo, Z., Wilson, M., Zhang, M., Cheng, Z. & Zhang, L. Post-collisional, K-rich mafic magmatism in south Tibet: constraints on Indian slab-to-wedge transport processes and plateau uplift. *Contrib. Mineral. Petrol.* **165(6)**, 1311-1340(2013).

28. Replumaz, A., Kárason, H., Hilst, R. D. V. D., Besse, J. & Tapponnier, P. 4-D evolution of SE Asia's mantle from geological reconstructions and seismic tomography. *Earth Planet. Sci. Lett.* **221(1)**, 103-115(2004).

29. Replumaz, A., Capitanio, F. A., Guillot, S., Negredo, A. M. & Villaseñor, A. The coupling of Indian subduction and Asian continental tectonics. *Gondwana Res.* **26(2)**, 608-626(2014).

30. Kosarev, G., Kind, R., Sobolev, S. V., Yuan, X., Hanka, W. & Oreshin, S. Seismic evidence for a detached Indian lithospheric mantle beneath Tibet. *Science* **283(5406)**, 1306-1309 (1999).

31. Scholl, D. W. & Huene, R. V. Crustal recycling at modern subduction zones applied to the past-Issues of growth and preservation of continental basement crust, mantle geochemistry, and supercontinent reconstruction. *4-D Framework of Continental Crust*, 9-32 (2007).

32. Jackson et al. The return of subducted continental crust in Samoan lavas. *Nature* **448(7154)**, 684-7 (2007).

Methods

Phase equilibria modelling and density calculation. Here we use the version 6.8.5 of Perple_X software package[33] to compute the phase relations and density evolution of continental crust, bulk oceanic crust (BOC) and pyrolite. Pseudosection calculations are based on the revised internally consistent thermodynamic data of Holland et al (2013)[34] for continental crust, and Xu et al (2008)[35] for bulk oceanic crust and pyrolite. The global average rock compositions (Extended Data Table 3) are chosen for the calculations of pseudosections and densities. The compositions of UCC and MCC are normalized in the NCKFMAS (Na_2O–CaO–K_2O–FeO–MgO–Al_2O_3–SiO_2) model system, and the composition of LCC, BOC and pyrolite are normalized in the NCFMAS (Na_2O–CaO–FeO–MgO–Al_2O_3–SiO_2) model system. The simplified compositions used in phase equilibrium modelling are shown in Extended Data Table 3. The solid solution models include garnet (gt)[34,35], clinopyroxene (cpx)[34,35], orthopyroxene (opx) [34,35] and its high-P polymorph (C2/c)[34], wadsleyite (wad) [34,35], ringwoodite (ring) [34,35], CaSi-perovskite (ca-pv) [34,35], wuestite (wus)[35], plagioclase (pl) [34], kalsilite (kls) [34], microcline (mic) [34], K-wadeite (wa)[34], K-hollandite (hol) [34], corundum (cor) [34,35], spinel (sp) [34,35] and melt[34]. Quartz (qtz), coesite (coe), stishovite (stv), kyanite (ky) are treated as pure end-member phases. The software and thermodynamic data used to generate the phase diagrams can be downloaded from http://www.perplex.ethz.ch/.

Petrological-thermo-mechanical model configuration. The 2D large-scale numerical model is conducted in a Cartesian box of 5000×670 km and discretized using an Eulerian grid of 1397×267 nodes with variable spacing. The original model consists of a subducting continental plate of 2650 km, an overlying continental plate of 1650 km and an oceanic plate of 700 km in

between. The continental lithosphere is set up with a 23-km-thick felsic crust (12 km UCC and 11 km MCC), a 17-km-thick mafic LCC[10] and a mantle layer. The oceanic lithosphere is composed of a 2-km-thick basaltic upper OC, a 5-km-thick gabbroic lower OC and a mantle layer with the thickness dependent on the age of lithosphere. A narrow weak zone with wet-olivine rheology is applied between the subducting oceanic and overlying continental plates to localize the initial convergence. A 10-km-thick 'stick air' layer with low density and viscosity is set above the crust in order to mimic a pseudo free surface condition[36,37].

The velocity boundary conditions are free slip at the left, right, and top boundaries. The lower boundary is treated as a mass-conversation preamble boundary for the purpose of satisfying free slip at about 1000 km below the base of the model (external lower boundary)[38]. Details of external lower boundary are provided elsewhere[38]. The original model (Fig. 2a) is pushed internally by a constant convergence velocity of 10 cm/yr for 7 Myrs, with a total convergence of 700 km. It leads to a scenario with the beginning of continental collision (Fig. 2b), after which the convergence velocity is cancelled, leaving the collisional process driven purely by the internal buoyancy.

The initial temperature structure of oceanic lithosphere is defined by the half-space cooling model[22]. For continental plate, a linear temperature gradient is applied with 0°C at the surface and 1350 °C at the bottom of lithospheric mantle (Fig. 2a). An adiabatic temperature gradient of 0.5°C/km is applied for sub-lithospheric mantle. The temperature boundary conditions have a fixed value (0°C) for the upper boundary and zero horizontal heat flux across the side boundaries. An infinity-like external constant temperature is imposed in the lower thermal boundary, which allows both temperatures and vertical heat fluxes to vary along the permeable lower boundary[38].

405

406 **Petrological-thermo-mechanical modelling approach.** The calculated density database is
407 further integrated into the 2-D thermo-mechanical numerical code I2VIS, which is based on
408 finite-difference method and marker-in-cell technique[18,19]. The fundamental equations of the
409 numerical model include the conservation equations of mass, momentum and energy (1)-(3).

410 $$\frac{\partial \mathrm{v}_i}{\partial \mathrm{x}_i} = 0 \qquad (1)$$

411 $$\frac{\partial \sigma'_{ij}}{\partial \mathrm{x}_j} - \frac{\partial P}{\partial \mathrm{x}_i} = -\rho g_i \qquad (2)$$

412 $$\rho C_p \left(\frac{DT}{Dt}\right) = \frac{\partial}{\partial \mathrm{x}_i}\left(k \frac{\partial T}{\partial \mathrm{x}_i}\right) + H_r + H_a + H_S + H_L \qquad (3)$$

413 where v is velocity, x_i coordinate, σ' the deviatoric stress tensor, P dynamic pressure, ρ effective
414 density, g gravitational acceleration, C_p heat capacity, T temperature, k thermal conductivity, H_r
415 radioactive heating, H_a adiabatic heating, H_S shear heating, and H_L latent heating. Complete
416 details of the numerical method are provided elsewhere[18,19].

417 Two different density models are applied and compared in the numerical simulations. In
418 the first model, the density is linearly dependent on pressure and temperature, but does not
419 include any phase transition. Thus, the effective density for a specific rock type can be calculated
420 according to the equation (4)

421 $$\rho(P,T) = \rho_0[1 - \alpha(T - T_0)][1 + \beta(P - P_0)] \qquad (4)$$

422 where ρ_0 is the standard density under the reference condition with P_0=0.1 MPa and T_0=298 K;
423 α the thermal expansion coefficient and β the compressibility coefficient (Extended Data Table
424 6). Alternatively, the second model incorporates our calculated density database with multiple
425 phase transitions and density jumps obtained from Perple_X (Extended Data Fig. 1), including

the remarkable phase transition boundaries at 410 km and 660 km discontinuities. The effective density is thus a complex, non-linear function of temperature, pressure and composition ($\rho = f(P, T, C_m)$).

The combined visco-plastic rheology is employed in the numerical model to describe the rock mechanical behavior[18]. The viscosity of rocks deforming by dislocation creep is defined as

$$\eta_{ductile} = (\dot{\varepsilon}_{II})^{\frac{1-n}{n}} (A_D)^{-\frac{1}{n}} \exp\left(\frac{E+PV}{nRT}\right) \quad (5)$$

where $\dot{\varepsilon}_{II}$ is the second invariant of the strain rate tensor, A_D (preexponential factor), E (activation energy), V (activation volume), and n (creep exponent) are experimentally determined flow law parameters[39,40,41,42,43] as listed in Extended Data Table 5. The parameter R is the gas constant.

We combine the viscous rheology with an extended Drucker-Prager yield criterion[43] to simulate the visco-plastic behavior of the rocks:

$$\eta_{plastic} = \frac{\sigma_{yield}}{2\dot{\varepsilon}_{II}} \quad (6)$$

$$\sigma_{yield} = C_0 + P\, sin(\varphi_{eff}) \quad (7)$$

where σ_{yield} is the yield stress, P dynamic pressure, C_0 the residual rock strength at $P = 0$; φ_{eff} the effective internal friction angle (Extended Data Table 6).

The integrated viscosity of ductile and plastic deformation is the minimum value of them[43].

$$\eta_{eff} = min(\eta_{ductile}, \eta_{plastic}) \quad (8)$$

Analytical model for subducting slab pull quantification. In the simplified subduction model, a continental lithosphere is subducting following the preceding oceanic slab to the maximum depth of 660 km. The continental slab includes a 12-km-thick UCC, an 11-km-thick MCC and a

17-km-thick LCC, according to the global average thickness of crust[10], as well as a subjacent lithospheric mantle (LM). The oceanic slab consists of a 7-km-thick OC and the subjacent lithospheric mantle. The possible composition-induced density contrast between the continental/oceanic lithospheric mantle and the surrounding mantle is ignored for simplicity. The model geometry is shown in Fig. 3a, with a high resolution of 300 m × 300 m. The analytical model of the subduction-zone thermal structure is calculated from Davies (1999)[21] and shown below:

$$T_{(x,y)} = T_1 + \left(\frac{T_1 - T_0}{h}\right)\left\{\left(\frac{x-h}{2}\right)\left[erf\left(-\frac{x-h}{\sqrt{4\kappa y/v}}\right) - erf\left(-\frac{x}{\sqrt{4\kappa y/v}}\right)\right]\right.$$

$$\left. - \left(\sqrt{\frac{\kappa y}{v\pi}}\right)\left[erf\left(-\left(\frac{x-h}{\sqrt{4\kappa y/v}}\right)^2\right) - erf\left(-\left(\frac{x}{\sqrt{4\kappa y/v}}\right)^2\right)\right]\right\}$$

$$+ \left(\frac{T_1 - T_0}{d}\right)\left\{\left(\frac{x+d}{2}\right)\left[erf\left(-\frac{x+d}{\sqrt{4\kappa y/v}}\right) - erf\left(-\frac{x}{\sqrt{4\kappa y/v}}\right)\right]\right.$$

$$\left. - \left(\sqrt{\frac{\kappa y}{v\pi}}\right)\left[erf\left(-\left(\frac{x+d}{\sqrt{4\kappa y/v}}\right)^2\right) - erf\left(-\left(\frac{x}{\sqrt{4\kappa y/v}}\right)^2\right)\right]\right\} \quad (9)$$

where T_1 is the mantle potential temperature, T_0 is the initial minimum temperature on the slab, h the lithosphere thickness, κ the thermal diffusivity, v the convergence velocity, d the initial thickness of the boundary layer in the mantle wedge, and *erf* the error function.

For a specific position (x, y), the lithostatic pressure $P_{(x,y)}$ is given by

$$P_{(x,y)} = \rho g(x \sin\theta + y \cos\theta) \quad (10)$$

where θ is the subduction angle. The slab density, $\rho_{(x,y)}$, is a function of $T_{(x,y)}$, $P_{(x,y)}$ and the composition C_m:

$$\rho_{(x,y)} = f\left(P_{(x,y)}, T_{(x,y)}, C_m\right) \quad (11)$$

where C_m = UCC, MCC, LCC, MORB, or LM.

Based on the above density structure, the total negative buoyancy force of the descending CC (F_{CC}) is obtained by integrating the density contrast $\Delta\rho_{(x,y,C_m)}$ in two dimensions on the vertical section of the subducted CC (Fig. 3b):

$$F_{CC} = \int_0^{L_C}\int_0^{T_{UCC}} \left(\rho_{(x,y,C_{UCC})} - \rho_m\right) g \sin\theta \, dxdy + \int_0^{L_C}\int_{T_{UCC}}^{T_{MCC}} \left(\rho_{(x,y,C_{MCC})} - \rho_m\right) g \sin\theta \, dxdy + \int_0^{L_C}\int_{T_{MCC}}^{T_{LCC}} \left(\rho_{(x,y,C_{LCC})} - \rho_m\right) g \sin\theta \, dxdy \quad (12)$$

where L_C is the length of the subducted CC after the transition from oceanic subduction to continental collision, and L_C increases from 0 to $\frac{660}{\sin\theta}$ km; T_{UCC}, T_{MCC}, and T_{LCC} are the thicknesses of UCC, MCC and LCC, respectively, with $T_{UCC} = 12\ km, T_{MCC} = 23\ km, T_{LCC} = 40\ km$; ρ_m is the density of the surrounding rock derived from PREM[44]. These three terms on the right-hand side define the slab pull of UCC, MCC, LCC, respectively, which are further named as F_{UCC}, F_{MCC}, and F_{LCC}. Accordingly, the slab pull of the conjoint OC above 660D (F_{OC}) is expressed as:

$$F_{OC} = \int_{L_{CC}}^{660} \left\{ \int_0^{T_{OC}} \left(\rho_{(x,y,C_{OC})} - \rho_m\right) g \sin\theta \, dx \right\} dy \quad (13)$$

where T_{OC} is the thickness of OC, with $T_{OC} = 7\ km$ in this study.

Code availability

The open-sourced software Perple_X and thermodynamic data can be downloaded from http://www.perplex.ethz.ch/. The I2VIS code associated with this paper should be requested from the main code developer (*taras.gerya@erdw.ethz.ch*). The petrological dataset and the computer code used for analytical calculation of slab pull are available from the authors.

Data availability

The data supporting the finding of this study are available within the paper (including Methods and Extended Data).

33. Connolly, J. A. D. Computation of phase equilibria by linear programming: A tool for geodynamic modeling and its application to subduction zone decarbonation. *Earth Planet. Sci. Lett.* 236(1), 524-541 (2005).
34. Holland T. J. B., Hudson N. F .C., Powell R & Harte B. New thermodynamic models and calculated phase equilibria in NCFMAS for basic and ultrabasic compositions through the transition zone into the uppermost lower mantle. *J PETROL* 54(9), 1901-1920 (2013).
35. Xu, W., Lithgow-Bertelloni, C., Stixrude, L., Ritsema, J. The effect of bulk composition and temperature on mantle seismic structure. *Earth Planet. Sci. Lett.* 275(1-2), 0-79 (2008).
36. Schmeling, H. et al. A benchmark comparison of spontaneous subduction models—Towards a free surface. *Phys. Earth Planet. Inter.* 171(1-4), 198-223 (2008).
37. Crameri, F. et al. A comparison of numerical surface topographycalculations in geodynamic modelling: An evaluation of the “sticky air” method. Geophys. J. Int. 189(1), 38–54 (2012).
38. Li, Z. H., Liu, M., & Gerya, T. Lithosphere delamination in continental collisional orogens: A systematic numerical study. *J. Geophys. Res. Solid Earth* 121, 5186–5211 (2016).
39. Kirby, S. H. Rheology of the lithosphere. *Rev. Geophys. Space Phys.* 21, 1458–1487 (1983).
40. Kirby, S. H. & Kronenberg A. K. Rheology of the lithosphere: Selected topics. *Rev. Geophys*. 25, 1219–1244 (1987).
41. Ranalli, G. &. Murphy, D. C. Rheology stratification of the lithosphere. *Tectonophysics* 132, 281–295 (1987).
42. Ji, S. & Zhao, P. Flow laws of multiphase rocks calculated from experimental data on the constituent phases. *Earth Planet. Sci. Lett.* 117, 181–187 (1993).
43. Ranalli, G. Rheology of the Earth, Deformation and flow process in geophysics and geodynamics. -2rd edition (1995).
44. Dziewonski, A. M. & Anderson, D. L. Preliminary reference earth model. *Phys. Earth Planet. Inter.* 25(4), 297-356 (1981).

Acknowledgements

We acknowledge the financial support from the National Natural Science Foundation of China (91755206, 41520104004, 41774108, 91855208). T. Gerya and J. Connolly are thanked for fruitful discussion.

Author Contributions

L.F.Z. and Z.H.L conceived the study. Y.W. performed the density modelling and analytical calculation of slab pull. Y.W. and Z.H.L conducted the 2D petrological-thermo-mechanical models. All authors analysed the data, discussed the results and contributed to writing the paper.

Competing interests The authors declare no competing interests.

Supplementary Files

This is a list of supplementary files associated with this preprint. Click to download.

- Extendeddatafiguresandtables.docx
- Fig.S1.jpg
- Fig.S2.jpg
- Fig.S3.jpg
- Fig.S4.jpg
- Fig.S5.jpg
- Fig.S6.jpg
- Fig.S7.jpg